Article

# Noncovalently Connected Micelles, Nanoparticles, and Metal-Functionalized Nanocages Using Supramolecular Self-Assembly

Adam O. Moughton, and Rachel K. O'Reilly

*J. Am. Chem. Soc.*, **2008**, 130 (27), 8714-8725 • DOI: 10.1021/ja800230k • Publication Date (Web): 13 June 2008



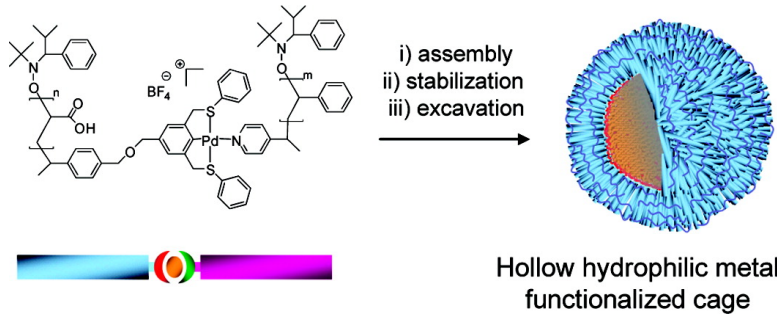


## More About This Article

Additional resources and features associated with this article are available within the HTML version:

- Supporting Information
- Links to the 1 articles that cite this article, as of the time of this article download
- Access to high resolution figures
- Links to articles and content related to this article
- Copyright permission to reproduce figures and/or text from this article

View the Full Text HTML

J|A|C|S
ARTICLES

Published on Web 06/13/2008

# Noncovalently Connected Micelles, Nanoparticles, and Metal-Functionalized Nanocages Using Supramolecular Self-Assembly

Adam O. Moughton and Rachel K. O'Reilly*

*Melville Laboratory for Polymer Synthesis, Department of Chemistry, University of Cambridge, Lensfield Road, Cambridge CB2 1EW, United Kingdom*

Received January 10, 2008; E-mail: rko20@cam.ac.uk

***Abstract:*** An SCS "pincer"-based nitroxide-mediated polymerization (NMP) initiator has been synthesized and utilized to polymerize *tert*-butyl acrylate ($^t$BuA), affording polymers with control over molecular weight and polydispersity. $^1$H NMR spectroscopy indicates that the sulfur end group remains intact after deprotection of the P$^t$BuA segment to yield a poly(acrylic acid) segment. The hydrophilic polymer-tethered SCS ligand has been demonstrated to bind to palladium(II), as characterized by a distinctive Pd−C shift in the $^{13}$C NMR spectrum and a diagnostic metal-to-ligand charge-transfer band in the UV−vis spectrum. A pyridine-functionalized NMP initiator has also been synthesized and used to initiate the NMP of styrene with good control and end group fidelity. The binding of these two chain end ligand-functionalized polymers to form an amphiphilic metallosupramolecular diblock copolymer is facile, as indicated through extended $^1$H and $^{13}$C NMR studies. The self-assembly of this diblock into well-defined, monodisperse, noncovalently connected micelles (NCCMs) is reported and has been characterized by dynamic light scattering, transmission electron microscopy, and atomic force microscopy. The NCCMs were selectively stabilized throughout the shell layer to produce stable noncovalently connected nanoparticles, resulting in a distinctive reduction in the solution hydrodynamic radius and zeta potential compared to those of the precursor micelle. The hydrophobic core domain was then readily removed via dialysis at low pH to afford a hollow polymeric nanocage with well-defined interior functionality. A significant increase in the solution hydrodynamic radius and shape by AFM analysis was observed upon removal of the core, and the hydrophilic nanocages were shown to be ineffective in the sequestration of hydrophobic dye molecules relative to the parent nanoparticle.

## 1. Introduction

The term "supramolecular" encompasses many chemical and biological systems; by definition, these systems exhibit the association of several molecules, which are held together by intermolecular forces. Supramolecular structures are constructed through a delicate balance between strong covalent bonds that hold the molecular building blocks together and the reversible intermolecular forces that assemble them. These reversible, cohesive forces are comparatively weak, noncovalent interactions[1] and include van der Waals forces, hydrogen and metal-to-ligand bonding, electrostatic forces, hydrophobic−hydrophilic interactions, and $\pi-\pi$ stacking. Noncovalent interactions between molecules impart an extra form of hierarchal assembly and organization upon the system to afford various well-defined supramolecular structures, on a larger scale than that of their component parts.[2,3] This organization or energy minimization of the system is termed "self-assembly".[1] Nature uses the unique power of this self-assembly process to construct the elegant supramolecular architectures seen in biological systems. In recent years, researchers have tried to mimic the kind of structural complexity found in Nature in their design of synthetic nanoscaled assemblies for utilization as new materials with desirable functions and properties.[4–12]

To this end, the designed manipulation of noncovalent interactions between specifically chosen organic molecules, or in particular polymers, is a powerful assembly tool.[13] This strategy has been exploited for polymeric systems in recent years via the incorporation of H-bonding motifs and metal−ligand binding sites by many research groups, but in particular those of Meijer,[14–18] Schubert,[19–28] Weck,[29–37] ten Brinke,[38–40] and

(1) Lehn, J.-M. *Angew. Chem., Int. Ed.* **1990**, *29*, 1304–1319.
(2) Hoeben, F. J. M.; Jonkheijm, P.; Meijer, E. W.; Schenning, A. P. H. J. *Chem. Rev.* **2005**, *105*, 1491–1546.
(3) Svikova, S.; Rowan, S. J. *Chem. Soc. Rev.* **2005**, *34*, 9–21.
(4) Zhang, Q.; Remsen, E. E.; Wooley, K. L. *J. Am. Chem. Soc.* **2000**, *122*, 3642–3651.
(5) Fyfe, M. C. T.; Stoddart, J. F. *Acc. Chem. Res.* **1997**, *30*, 393–401.
(6) Vriezema, D. M.; Comellas Aragones, M.; Elemans, J. A. A. W.; Cornelissen, J. J. L. M.; Rowan, A. E.; Nolte, R. J. M. *Chem. Rev.* **2005**, *105*, 1445–1490.
(7) O'Reilly, R. K.; Hawker, C. J.; Wooley, K. L. *Chem. Soc. Rev.* **2006**, *35*, 1068–1083.
(8) Hawker, C. J.; Wooley, K. L. *Science* **2005**, *309*, 1200–1205.
(9) Brunseld, L.; Folmer, B. J. B.; Sijbesma, R. P.; Meijer, E. W. *Chem. Rev.* **2001**, *101*, 4071–4097.
(10) Hamley, I. M. *Soft Matter* **2005**, *1*, 36–43.
(11) Sherrington, D. C.; Taskinen, K. A. *Chem. Soc. Rev.* **2001**, *30*, 83–93.
(12) Lutkenhaus, J. L.; Hrabak, K. D.; McEnnis, K.; Hammond, P. T. *J. Am. Chem. Soc.* **2005**, *127*, 17228–17234.
(13) Ciferri, A. *Macromol. Rapid Commun.* **2002**, *23*, 511–529.
(14) Sijbesma, R. P.; Beijer, F. H.; Brunsveld, L.; Folmer, B. J. B.; Hirschberg, J. H. K. K.; Lange, R. F. M.; Lowe, J. K. L.; Meijer, E. W. *Science* **1997**, *278*, 1601–1604.


**10.1021/ja800230k CCC: $40.75** 

Rowan.[41–43] To date, the most promising and facile route toward nanosized and utilizable assemblies involves the self-assembly of polymers into vesicle or micelle-type structures.[44–50] To enable phase-separated self-assembly, amphiphilic diblock copolymers must be used, i.e., those which contain hydrophobic and hydrophilic segment(s), which can mimic natural phospholipids and form supramolecular structures with predictable morphologies.[51,52]

The micellization of amphiphilic diblock copolymers in a solvent that is selective for one of the blocks, in which the two different polymer chains are covalently connected at their junction, is the most common way to produce such assemblies.[7,53] It has also been shown in recent years by a number of research groups that dynamic micelle structures formed from such diblock copolymers can be covalently stabilized throughout their core or shell domain using polymerization techniques, alkylation, or amidation chemistry to afford robust cross-linked nanoparticles.[54–61] From these nanoparticle scaffolds, it has been demonstrated that permeable, water-filled, cage-like nanostructures can be formed upon core removal, using either ozonolytic or hydrolytic degradation chemistry.[4,56,62] The utilization of a nanoparticle template for the construction of nanocages has advantages, such as the well-defined and robust nature of the resultant cage-like structures, although the harsh excavation chemistries employed can lead to nanocage degradation or loss of reactive functionality within the interior.[63–66]

Strategies toward the synthesis of micelle structures can be "block-copolymer-free", i.e., by the incorporation of diblock copolymers that are noncovalently linked at their homopolymer chain end by specific intermolecular interactions such as H-bonding or metal−ligand interactions. The analogous nanostructures formed from such polymers are often termed "noncovalently connected micelles" (NCCMs), and this approach was pioneered by Jiang and co-workers, who have synthesized micelles and nanocages from a range of H-bonding motifs using noncovalently connected amphiphilic diblock copolymers.[67–72]

Metal−ligand coordination is a particularly interesting noncovalent motif to incorporate onto polymers since the bonding is highly directional and its relative strength can be readily tuned—as a result, chemists can take advantage of a whole host of well-studied metal−ligand combinations.[73] For example, Weck and co-workers have shown that specific metal−ligand interactions can enhance the self-assembly of polymeric


(15) Lange, R. F. M.; Meijer, E. W. *Macromolecules* **1995**, *28*, 782–783.
(16) Brunsveld, L.; Vekemans, J. A. J. M.; Hirschberg, J. H. K. K.; Sijbesma, R. P.; Meijer, E. W. *Proc. Natl. Acad. Sci. U.S.A.* **2002**, *99*, 4977–4982.
(17) Sijbesma, R. P.; Meijer, E. W. *Chem. Commun.* **2003**, 5–16.
(18) van Gorp, J. J.; Vekemans, J. A. J. M.; Meijer, E. W. *Chem. Commun.* **2004**, 60–61.
(19) Schubert, U. S.; Eschbaumer, C. *Macromol. Symp.* **2001**, *163*, 177–188.
(20) Schubert, U. S.; Heller, M. *Chem.-Eur. J.* **2001**, *7*, 5252–5259.
(21) Gohy, J. F.; Lohmeijer, B. G. G.; Schubert, U. S. *Macromolecules* **2002**, *35*, 4560–4563.
(22) Gohy, J.-F.; Lohmeijer, B. G. G.; Alexeev, A.; Wang, X.-S.; Manners, I.; Winnik, M. A.; Schubert, U. S. *Chem.-Eur. J.* **2004**, *10*, 4315–4323.
(23) Hoogenboom, R.; Schubert, U. S. *Chem. Soc. Rev.* **2006**, *35*, 622–629.
(24) Chiper, M.; Meier, M. A. R.; Kranenburg, J. M.; Schubert, U. S. *Macromol. Chem. Phys.* **2007**, *208*, 679–689.
(25) Schubert, U. S. *Synth. Met.* **2001**, *121*, 1249–1252.
(26) Lohmeijer, B. G. G.; Schlaad, H.; Schubert, U. S. *Macromol. Symp.* **2003**, *196*, 125–135.
(27) Lohmeijer, B. G. G.; Schubert, U. S. *J. Polym. Sci. Part A: Polym. Chem.* **2005**, *43*, 6331–6344.
(28) Fustin, C.-A.; Guillet, P.; Schubert, U. S.; Gohy, J. F. *Adv. Mater.* **2007**, *19*, 1665–1673.
(29) Pollino, J. M.; Weck, M. *Org. Lett.* **2002**, *4*, 753–756.
(30) Pollino, J. M.; Stubbs, L. P.; Weck, M. *Macromolecules* **2003**, *36*, 2230–2234.
(31) Pollino, J. M.; Weck, M. *Synthesis* **2002**, 1277–1285.
(32) Carlise, J. R.; Weck, M. *J. Polym. Sci. Part A: Polym. Chem.* **2004**, *42*, 2973–2984.
(33) Pollino, J. M.; Stubbs, L. P.; Weck, M. *J. Am. Chem. Soc.* **2004**, *126*, 563–567.
(34) Yu, K.; Sommer, W.; Weck, M.; Jones, C. W. *J. Cat.* **2004**, *226*, 101–110.
(35) Sommer, W. J.; Yu, K.; Sears, J. S.; Ji, Y.; Zheng, X.; Davis, R. J.; Sherrill, C. D.; Jones, C. W.; Weck, M. *Organometallics* **2005**, *24*, 4351–4361.
(36) Yu, K.; Sommer, W.; Richardson, J. M.; Weck, M.; Jones, C. W. *Adv. Synth. Catal.* **2005**, *347*, 161–171.
(37) South, C. R.; Higley, M. N.; Leung, K. C. F.; Lanari, D.; Nelson, A.; Grubbs, R. H.; Stoddart, J. F.; Weck, M. *Chem.-Eur. J.* **2006**, *12*, 3789–3797.
(38) de Moel, K.; Alberda van Ekenstein, G. O. R.; Nijland, H.; Polushkin, E.; ten Brinke, G. *Chem. Mater.* **2001**, *13*, 4580–4583.
(39) Ruokolainen, J.; Saariaho, M.; Ikkala, O.; ten Brinke, G. *Macromolecules* **1999**, *32*, 1152–1158.
(40) Stepanyan, R.; Subbotin, A.; Knaapila, M.; Ikkala, O.; ten Brinke, G. *Macromolecules* **2003**, *36*, 3758–3763.
(41) Beck, J. B.; Ineman, J. M.; Rowan, S. J. *Macromolecules* **2005**, *38*, 5060–5068.
(42) Weng, W.; Beck, J. B.; Jamieson, A. M.; Rowan, S. J. *J. Am. Chem. Soc.* **2006**, *128*, 11663–11672.
(43) Sivakova, S.; Bohnsack, D. A.; Mackay, M. E.; Suwanmala, P.; Rowan, S. J. *J. Am. Chem. Soc.* **2005**, *127*, 18202–18211.
(44) Meier, W. *Chem. Soc. Rev.* **2000**, *29*, 295–303.
(45) Read, E. S.; Armes, S. P. *Chem. Commun.* **2007**, 3021–3035.
(46) Klok, H.-A.; Lecommandoux, S. *Adv. Mater.* **2001**, *13*, 1217–1229.
(47) Discher, D. E.; Eisenberg, A. *Science* **2002**, *297*, 967–973.
(48) Lodge, T. P. *Macromol. Chem. Phys.* **2003**, *204*, 265–273.
(49) Webber, S. E. *J. Phys. Chem. B* **1998**, *102*, 2618–2626.
(50) Zhang, L. F.; Eisenberg, A. *J. Am. Chem. Soc.* **1996**, *118*, 3168–3181.
(51) Lowik, D. W. P. M.; van Hest, J. C. M. *Chem. Soc. Rev.* **2004**, *33*, 234–245.
(52) Rodriguez-Hernandez, J.; Lecommandoux, S. *J. Am. Chem. Soc.* **2005**, *127*, 2026–2027.
(53) Reiss, G. *Prog. Polym. Sci.* **2003**, *28*, 1107–1170.
(54) Wooley, K., L. *J. Polym. Sci. Part A: Polym. Chem.* **2000**, *38*, 1397–1407.
(55) Thurmond, K. B.; Kowalewski, T.; Wooley, K. L. *J. Am. Chem. Soc.* **1996**, *118*, 7239–7240.
(56) Huang, H.; Remsen, E. E.; Kowalewski, T.; Wooley, K. L. *J. Am. Chem. Soc.* **1999**, *121*, 3805–3806.
(57) Butun, V.; Billingham, N. C.; Armes, S. P. *J. Am. Chem. Soc.* **1998**, *120*, 12135–12136.
(58) Ding, J. F.; Liu, G. J. *Macromolecules* **1998**, *31*, 6554–6558.
(59) Henselwood, F.; Liu, G. J. *Macromolecules* **1997**, *30*, 488–493.
(60) Liu, S.; Armes, S. P. *J. Am. Chem. Soc.* **2001**, *123*, 9910–9911.
(61) Sumerlin, B. S.; Lowe, A. B.; Thomas, D. B.; Convertine, A. J.; Donovan, M. S.; McCormick, C. L. *J. Polym. Sci. Part A: Polym. Chem.* **2004**, *42*, 1724–1734.
(62) Turner, J. L.; Wooley, K. L. *Nano Lett.* **2004**, *4*, 683–688.
(63) Cheng, C.; Qi, K.; Khoshdel, E.; Wooley, K. L. *J. Am. Chem. Soc.* **2006**, *128*, 6808–6809.
(64) Ma, Q.; Remsen, E. E.; Kowalewski, T.; Schaefer, J.; Wooley, K. L. *Nano Lett.* **2001**, *1*, 651–655.
(65) Sanji, T.; Nakatsuka, Y.; Ohnishi, S.; Sakurai, H. *Macromolecules* **2000**, *33*, 8524–8526.
(66) Turner, J. L.; Chen, Z.; Wooley, K. L. *J. Controlled Release* **2005**, *109*, 189–202.
(67) Yuan, X.; Jiang, M.; Zhao, H.; Wang, M.; Zhao, Y.; Wu, C. *Langmuir* **2001**, *17*, 6122–6126.
(68) Chen, D.; Jiang, M. *Acc. Chem. Res.* **2005**, *38*, 494–502.
(69) Wang, M.; Zhang, G.; Chen, D.; Jiang, M.; Liu, S. *Macromolecules* **2001**, *34*, 7172–7178.
(70) Zhao, H.; Liu, S.; Jiang, M.; Yuan, X. F.; An, Y.; Liu, L. *Polymer* **2000**, *41*, 2705–2709.
(71) Zhang, Y.; Xiang, M.; Jiang, M.; Wu, C. *Macromolecules* **1997**, *30*, 6084–6089.
(72) Wang, M.; Jiang, M.; Ning, F.; Chen, D.; Liu, S.; Duan, H. *Macromolecules* **2002**, *35*, 5980–5989.
(73) Kurth, D. G.; Higiuchi, M. *Soft Matter* **2006**, *2*, 915–927.

systems.[31–33,74] Their elegant work has utilized the catalytic potential of metal complexes on a polymer support, notably for an SCS "pincer"−Pd(II) complex system for use in Heck catalysis.[34–36] The complexation of this Pd(II)−SCS complex motif is also well known with pyridine, nitrile, and phosphine functionalities.[29–34,75–78] Schubert and co-workers have recently pioneered the application of synthetic strategies toward metallopolymer NCCMs using metal−ligand interactions.[21,22] In recent years, Schubert and co-workers have demonstrated that the incorporation of terpyridine ligands onto polymer chain ends enables access to an interesting block copolymer architecture, a metallosupramolecular diblock copolymer, via bis-complexation to ruthenium, among many other metals.[25–28] Moreover, through tailored selection of the polymer utilized to form the amphiphilic metallodiblock copolymer, supramolecular architectures such as metal-linked NCCMs can be achieved upon self-assembly.[21,22]

Recently, the preparation of tailor-made functionalized polymers for self-assembly has been markedly advanced by the developments in controlled radical polymerization (CRP) techniques. CRP allows for the synthesis of well-defined block copolymers with tunable molecular weights ($M_n$) and narrow polydispersities ($M_w/M_n$) for applications in self-assembly.[6] Moreover, CRP techniques such as reversible addition fragmentation chain transfer (RAFT)[79–82] and nitroxide-mediated polymerization (NMP)[83–86] allow for the preparation of chain-end-functionalized polymers via the prefunctionalization of the chain-transfer agent or initiator species, respectively. This concept has been used to synthesize a wide range of polymers bearing specifically targeted functional groups at their chain termini. For example, Hawker and co-workers showed that pendant end groups such as pyrene could be incorporated onto a range of different polymers prepared by NMP and the end groups were still present post-polymerization, thus demonstrating excellent polymerization end-group fidelity.[87] Schubert and co-workers have also made a significant contribution to this field by utilizing a terpyridine-functionalized NMP initiator capable of binding to a range of metal centers.[23,27] This functional initiator effectively mediates the controlled NMP of styrene, vinylpyridines, *N*′,*N*′-dimethylacrylamide, isoprene, and acrylates to obtain polymers with predictable $M_n$ and low $M_w/M_n$ that are valuable building blocks for utilization in the synthesis of metallosupramolecular polymer architectures.[27]

In this work, we describe the design and preparation of NCCMs which are self-assembled from an unsymmetrical supramolecular metallodiblock copolymer. An unsymmetrical binding unit was specifically chosen to join the two homopolymer blocks, to form the diblock, to allow for facile removal of one of the ligands to facilitate core removal. This strategy utlizes two ligand chain-end-functionalized homopolymers (of which one is hydrophobic and other is hydrophilic) which both undergo monocomplexation to a Pd(II) metal center to self-assemble to form an amphiphilic diblock copolymer. This metal complex at the interface between the two polymers utilizes the relatively weak coordination of a pyridine moiety to a Pd(II) metal center and a strongly bound SCS pincer ligand and represents the first report of an unsymmetrical metal−ligand interaction for the formation of a supramolecular block copolymer for self-assembly into micellar morphologies. This strategy relies upon the incorporation of the two complexing ligands onto the chain ends of two different polymer blocks. To achieve this goal and produce well-defined polymers with predictable molecular weights, NMP was used since we could readily synthesize two functional alkoxyamine NMP initiator species using well-established functionalization chemistries. The resultant end-functionalized, monodisperse polymers, with easily tunable molecular weights, were utilized to form well-defined supramolecular structures which could be readily tuned by tailoring the monomer to initiator ratios during polymer synthesis. These metallopolymers were then self-assembled to form well-defined micellar structures (NCCMs) which were stabilized throughout their shell domain to form robust and stable, noncovalently connected nanoparticles (NCCNs). Core removal of these NCCNs, by exhaustive dialysis at low pH, has been demonstrated to form hydrophilic, well-defined, cage-like nanostructures or nanocages via selective cleavage of the metal−hydrophobic chain bond while ensuring retention of the metal functionality within the interior of the nanostructure. Core removal exposes a nanostructure whose interior domain is functionalized with SCS pincer−Pd(II) complexes.

## 2. Experimental Section

**Materials.** Tetrahydrofuran (THF, 99%), methanol (99%), and all other chemicals were used as received from Aldrich, Fluka, and Acros unless otherwise stated. *tert*-Butyl acrylate and styrene monomers were distilled over $CaH_2$ prior to use and stored at −5 °C. 2,2,5-Trimethyl-4-phenyl-3-azahexane-3-oxy and *N*-*tert*-butyl-*O*-(1-(4-(chloromethyl)phenyl)ethyl)-*N*-(2-methyl-1-phenylpropyl)-hydroxylamine were synthesized as previously reported in the literature.[86] The pendant alcohol-functionalized SCS pincer ligand was synthesized as reported in the literature.[88] The palladium(II) precursor complex, $[Pd(PhCN)_2Cl_2]$, was synthesized according to a previously reported literature preparation.[89]

**Instrumentation.** Nuclear magnetic resonance (NMR) experiments ($^1H$ and $^{13}C$) were performed on a Bruker AVANCE 400 FT-NMR spectrometer using deuterated solvents. Coupling constants are in hertz, and chemical shifts are reported in parts per million relative to $CHCl_3$ (7.26 ppm for $^1H$ and 77.2 ppm for $^{13}C$) or DMSO-$d_6$ (2.50 ppm for $^1H$ and 39.52 ppm for $^{13}C$). Extended

(74) Nair, K. P.; Pollino, J. M.; Weck, M. *Macromolecules* **2006**, *39*, 931–940.
(75) van Manen, H.-J.; Nakashima, K.; Shinkai, S.; Kooijman, H.; Spek, A. L.; van Veggel, F. C. J. M.; Reinhoudt, D. N. *Eur. J. Inorg. Chem.* **2000**, *200*, 2533–2540.
(76) Bergbreiter, D. E.; Osburn, P. L.; Liu, Y. S. *J. Am. Chem. Soc.* **1999**, *121*, 9531–9538.
(77) Bergbreiter, D. E.; Osburn, P. L.; Wilson, A.; Sink, E. M. *J. Am. Chem. Soc.* **2000**, *122*, 9058–9064.
(78) Bergbreiter, D. E.; Osburn, P. L.; Frels, J. D. *Adv. Synth. Catal.* **2005**, *347*, 172–184.
(79) Moad, G.; Rizzardo, E.; Thang, S. H. *Aust. J. Chem.* **2005**, *58*, 379–410.
(80) Chiefari, J.; Chong, Y. K.; Ercole, F.; Krstina, J.; Jeffery, J.; Le, T. P. T.; Mayadunne, R. T. A.; Meijs, G. F.; Moad, C. L.; Moad, G.; Rizzardo, E.; Thang, S. H. *Macromolecules* **1998**, *31*, 5559–5562.
(81) Perrier, S.; Takolpuckdee, P. *J. Polym. Sci. Part A: Polym. Chem.* **2005**, *43*, 5347–5393.
(82) Takolpuckdee, P.; Westwood, J.; Lewis, D. M.; Perrier, S. *Macromol. Symp.* **2004**, *216*, 23–36.
(83) Hawker, C. J. *J. Am. Chem. Soc.* **1994**, *116*, 11185–11186.
(84) Hawker, C. J.; Barclay, G. G.; Orellana, A.; Dao, J.; Devonport, W. *Macromolecules* **1996**, *29*, 5245–5254.
(85) Hawker, C. J. *Acc. Chem. Res.* **1997**, *30*, 373–382.
(86) Benoit, D.; Chaplinski, V.; Braslau, R.; Hawker, C. J. *J. Am. Chem. Soc.* **1999**, *121*, 3904–3920.
(87) Rodlert, M.; Harth, E.; Rees, I.; Hawker, C. J. *J. Polym. Sci. Part A: Polym. Chem.* **2000**, *38*, 4749–4763.
(88) Meijer, M. D.; Mulder, B.; van Klink, G. P. M.; van Koten, G. *Inorg. Chim. Acta* **2003**, *352*, 247–252.
(89) Milani, B.; Marson, A.; Zangrando, E.; Mestroni, G.; Ernsting, J. M.; Elsevier, C. J. *Inorg. Chim. Acta* **2002**, *327*, 188–201.

$^1$H and $^{13}$C NMR spectra were recorded on an AVANCE 500 Cryo FT-NMR spectrometer, all at 25 °C.

Size exclusion chromatography/gel permeation chromatography (SEC/GPC) measurements were performed using a Viscotek VE1122 solvent delivery system with a Viscotek VE3580 RI detection system using THF as eluent at a flow rate of 1 mL/min, unless otherwise stated. The molecular weights of polymers were calculated relative to polystyrene or poly(methyl methacrylate) standards. UV−vis spectra were recorded on a Varian Cary 4000 UV−vis spectrophotometer in THF unless otherwise stated. Infrared spectroscopy was recorded on a Perkin-Elmer Precisely, Spectrum 100 FT-IR spectrometer.

Hydrodynamic diameters ($D_h$), size distributions, and zeta potentials ($\zeta$) for the micelles and nanoparticles in aqueous solutions were determined by dynamic light scattering (DLS). The DLS instrumentation consisted of a Malvern Zetasizer Nano ZS instrument operating at 25 °C with a 635-nm laser module. Measurements were made at a detection angle of 173° (back scattering), and Malvern DTS 4.00 software was utilized to analyze the data. All determinations were made in triplicate (with 12 runs recorded). Static light scattering (SLS) measurements were recorded on a Wyatt Dawn Helios II.

The height measurements and distributions for the nanoparticles were determined by tapping-mode atomic force microscopy (AFM) under ambient conditions in air. The sample solutions were prepared for AFM analysis by dilution (typical concentrations ca. 0.002 mg/mL) and deposition of a drop (2 $\mu$L) onto freshly cleaved mica and allowed to dry freely in air. The number-average particle heights ($H_{av}$) and diameter ($D_{av}$) values and standard deviations were generated from the sectional analysis of 100 particles from at least five different analysis regions.

TEM samples were diluted with a 1 wt % phosphotungstic acid stain (1:1). Carbon grids were prepared by argon plasma treatment to increase the surface hydrophilicity. Micrographs were collected at 64000× magnification unless otherwise stated. Histograms of number-average particle diameters ($D_{av}$) and standard deviations were generated from the analysis of a minimum of 150 particles from at least three different micrographs.

Mass spectra were acquired by matrix-assisted laser desorption/ionization time-of-flight (MALDI-ToF) mass spectrometry using a Bruker Daltonics Ultraflex II MALDI-ToF mass spectrometer, equipped with a nitrogen laser delivering 3-ns laser pulses at 337 nm. In general, solutions of dithranol as matrix, NaTFA as cationization agent, and polymer were prepared in THF at a concentration of 0.2 g/L. Ten-microliter aliquots of matrix, polymer, and NaTFA solutions were applied sequentially to the target, followed by solvent evaporation, to prepare a thin matrix/analyte film. The samples were measured in reflection ion mode in all cases.

**Synthesis of SCS NMP Initiator 1.** 3,5-Bis(phenylsulfidomethyl)benzyl alcohol[88] (1.00 g, 2.84 mmol) was dissolved in dry, degassed THF (10 mL) under a nitrogen atmosphere. NaH as a 60% dispersion in mineral oil (0.60 g, 14.9 mmol) was added, and the reaction mixture was stirred at room temperature for 30 min. The chloro-functionalized alkoxyamine initiator, *N*-*tert*-butyl-*O*-(1-(4-(chloromethyl)phenyl)ethyl)-*N*-(2-methyl-1-phenylpropyl)-hydroxylamine[86] (1.07 g, 2.84 mmol), was added as a solution in THF via cannular transfer, and the reaction was refluxed for 16 h under nitrogen. Upon the solution cooling to room temperature, acetic acid (ca. 5 mL) was added dropwise under nitrogen flow to decompose any excess sodium hydride. Dichloromethane (100 mL) was then added. The organic layers were washed with water (100 mL), sodium hydroxide (100 mL), and then a saturated brine solution (100 mL). The organic phase was dried over magnesium sulfate, filtered, and concentrated under vacuum. The crude product was purified by flash chromatography, eluting with 3:2 hexane/dichloromethane solution to give the product, **1** ($R_f$ = 0.5 in 3:2 hexane/dichloromethane) as a light-yellow gum, (0.82 g, 42%). $^1$H NMR ($CDCl_3$, 400 MHz): $\delta$ 7.43−7.09 (m, 22H, Ar*H*), 4.97 (br s, 1H, $CH_3CH$), 4.45 (s, 2H, $PhCH_2OCH_2$), 4.44 (s, 2H, $CH_2OCH_2Ph$), 4.02 (s, 4H, $CH_2SPh$), 3.51 (d, 1H, NC*H*, diastereoisomer A), 3.34 (d, 1H, NC*H*, diastereoisomer B), 2.44−2.39 (m, 1H, C*H*$(CH_3)_3$), 1.63 (d, 3H, diastereoisomer A), 1.58 (d, 3H, diastereoisomer B), 1.29 (d, 3H, diastereoisomer A), 1.09 (s, 9H, C(C$H_3)_3$, diastereoisomer A), 0.97 (d, 3H, diastereoisomer B), 0.85 (s, 9H, C(C$H_3$), diastereoisomer B), 0.59 (d, 3H, diastereoisomer A), 0.25 (d, 3H, diastereoisomer B). $^{13}$C NMR ($CDCl_3$, 400 MHz): $\delta$ 145.3, 142.5, 142.2, 138.9, 138.8 (Ar*C*), 137.9, 136.4, 136.1, 131.0, 128.8, 128.6, 127.7, 127.4, 127.2, 126.4, 126.3, 126.2, 126.2, 83.3, 82.5, 77.2, 72.2, ($CH_2OCH_2$) 72.1, ($CH_2OCH_2$) 71.4, 60.5, 38.9, 32.0, 31.7, 28.4, 24.7, 23.2, 22.7, 22.2, 22.0, 21.2, 15.2, 14.1. IR ($\nu_{max}$/cm$^{-1}$): 3058−2866 (C−H), 1583 (aromatic), 1480 (aromatic), 1360 (N−O), 1088 (C−O−C), 821 (1,3,5-trisubst. Ph ring). LC-MS: *m*/*z* 690.35 ($M^+$, 100%). C,H,N found: C, 76.63; H, 7.61; N, 2.05%. $C_{44}H_{51}NO_2S_2$ requires C, 76.59; H, 7.45; N, 2.03%.

**Synthesis of Pyridyl NMP Initiator 2.** A stream of air was bubbled through a mixture of toluene (125 mL) and ethanol (125 mL) for 1 h. 4-Vinylpyridine (3.58 g, 34.0 mmol), 2,2,5-trimethyl-4-phenyl-3-azahexane-3-oxy[86] (4.99 g, 22.7 mmol), (*R*,*R*)-(−)-*N*,*N*′-bis(3,5-di-*tert*-butylsalicylidene)-1,2-cyclohexane-diamine-managanese(III) chloride (2.06 g, 3.24 mmol), and sodium borohydride (1.72 g, 45.4 mmol) were then added, one immediately following the other. Air was bubbled through the mixture for 17 h. The reaction mixture was then filtered through silica gel in a sintered glass funnel and rinsed with dichloromethane followed by methanol. The filtrate was concentrated under vacuum and purified by flash chromatography, packed in dichloromethane, eluting with 20:1 dichloromethane/methanol ($R_f$ = 0.2) to yield the product as a light brown oil which crystallizes at −5 °C into a light brown crystalline solid, **2** (3.84 g, 52%). $^1$H NMR ($CDCl_3$, 400 MHz): $\delta$ 8.50−8.70 (br m, 2H, py-α-*H*), 7.45−7.30 (br m, 2H py-*β*-*H*), 7.29−7.11 (m, 5H, Ar*H*), 4.95−4.87 (m, 1H, $CH_3CH$), 3.43−3.33 (dd, 1H, NC*H*, diastereoisomer A), 2.34−2.25 (m, 1H, C*H*$(CH_3)_3$), 1.61 (d, 3H, diastereoisomer A), 1.55 (d, 3H, diastereoisomer B), 1.27 (d, 3H, diastereoisomer A), 1.05 (s, 9H, C(C$H_3)_3$, diastereoisomer A), 0.95 (d, 3H, diastereoisomer B), 0.80 (s, 9H, C(C$H_3$), diastereoisomer B), 0.54 (d, 3H, diastereoisomer A), 0.25 (d, 3H, diastereoisomer B). $^{13}$C NMR ($CDCl_3$, 400 MHz): $\delta$ 154.3, 153.5, 149.8 (Py-α-*C*), 142.1, 141.9, 130.5, 130.7, 127.5, 127.3, 126.5, 126.4, (Ar*C*), 82.5, 81.3, 77.0, 72.2, 60.7, 32.0, 28.4, 24.4, 23.0, 21.8. IR ($\nu_{max}$/cm$^{-1}$): 3038−2869 (C−H), 1598 (aromatic), 1482 (aromatic), 1362 (N−O), 1105 (C−N). LC-MS: *m*/*z* 326.5 ($M^+$, 100%). C,H,N found: C, 77.29; H, 9.36; N, 8.52%. $C_{21}H_{30}N_2O$ requires C, 77.26; H, 9.26; N, 8.58%.

**General Acrylate Polymerization Using 1.** *tert*-Butyl acrylate (1.5 g, 11.7 mmol), the SCS pincer alkoxyamine initiator **1** (0.162 g, 0.23 mmol), and 2,2,5-trimethyl-4-phenyl-3-azahexane-3-oxy (0.0052 g, 0.0234 mmol) were placed in an oven-dried ampule with a stirrer bar. The ampule was degassed three times and sealed under nitrogen, and the polymerizations were heated at 125 °C for 115 h. For lower conversions, shorter reaction times were used. The polymer was then dissolved in a minimum amount of THF and purified by precipitation into ice-cold methanol (repeated three times) and dried in a vacuum oven at room temperature overnight. SCS pincer chain-end-functionalized poly(*tert*-butyl acrylate) (P$^t$BuA) **3** was isolated as a white solid (0.62 g, 60%). $M_n^{NMR}$ = 4500 g/mol, $M_n^{GPC}$ = 5200 g/mol, $M_w/M_n$ = 1.14. IR ($\nu_{max}$/cm$^{-1}$): 2978, 2933, 1722, 1480, 1449, 1392, 1366, 1254, 1141, 1035, 909, 751. $^1$H NMR ($CDCl_3$, 500 MHz): $\delta$ 1.20−1.50 (br, ($CH_3)_3$C), 1.24−1.68 (br, $CH_2$ of the polymer backbone), 1.74−1.94 (br, $CH_2$ of the polymer backbone), 2.15−2.35 (br, C*H* of the polymer backbone), 4.05 (s, $CH_2SPh$ in end group), 4.41 (s, $CH_2OCH_2$ in end group), 4.42 (s, $CH_2OCH_2$ in end group), 7.11−7.27 (m, Ar*H* in end groups). $^{13}$C NMR ($CDCl_3$, 500 MHz): $\delta$ 21.2 ($CH_3CHCH_3$ on the chain end), 27.9−28.1 ((*C*$H_3)_3$C on the side chain), 35.7−37.2 (carbon on the polymer backbone), 41.7−42.2 (carbon on the polymer backbone), 80.2 ((CH$_3)_3C$ on the polymer side chain), 125.5−135.8 (Ar*C* on the chain ends), 173.6−173.8 (*C*=O on the polymer side chain).

**General Styrene Polymerization Using 2.** Styrene (3.03 g, 29.1 mmol) and the pyridyl ligand alkoxyamine initiator **2** (0.19 g, 0.582 mmol) were placed in an ampule with a stirrer bar. The ampule was degassed three times and sealed under nitrogen, and the polymerizations were heated at 125 °C for 12 h. For lower conversions, shorter reaction times were used. The polymer was then dissolved in a minimum amount of THF and purified by precipitation into a rapidly stirred solution of ice-cold methanol (repeated three times) and dried in a vacuum oven at 40 °C overnight. Pyridyl chain-end-functionalized polystyrene (PS) **4** was isolated as a white solid (1.59 g, 81% yield). $M_n^{NMR} = 3600$ g/mol, $M_n^{GPC} = 2400$ g/mol, $M_w/M_n = 1.18$. IR ($\nu_{max}$/cm$^{-1}$): 1598 (py), 1569 (py), 1584, 1515, 1443, 1394, 1362 (N−O), 1296, 1263, 1172, 1147, 1102, 1067, 1058, 1108, 939, 838, 823, 797, 763, 724, 704, 689, 655. $^1$H NMR ($CDCl_3$, 500 MHz): $\delta$ 1.22−1.70 (br, C$H_2$ of the polymer backbone), 1.74−2.04 (br, C$H_2$ of the polymer backbone), 2.15−2.41 (br, C*H* of the polymer backbone), 6.20−7.30 (m, Ar*H* in side chain), 7.11−7.27 (m, Ar*H* in end groups), 8.58 (m, α pyr. Ar*H*). $^{13}$C NMR ($CDCl_3$, 500 MHz): $\delta$ 149.5 (α pyr. Ar*C*), 131.0−122.5 (Ar*C* on side chain), 46.4−36.4 (carbons on the polymer backbone), 31.6, 30.9, 28.2, 21.2.

**Complexation of 3 with Pd(II) To Give Metal-Complexed P$^t$BuA 5.** Polymer **3** (0.050 g, 0.0097 mmol) was dissolved in acetonitrile (5 mL), and the solution was placed under nitrogen. The palladium precursor complex, $[Pd(MeCN)_4(BF_4)_2]$ (0.00517 g, 0.012 mmol), was added, and the mixture was stirred at room temperature for 24 h. After evaporation of the solvent under vacuum, **3** was redissolved in THF (1 mL) and purified by precipitation into methanol/water (4:1). The solvent was decanted off, and the polymer was redissolved in THF (ca. 100 mL), dried over magnesium sulfate, and filtered, and the solvent was removed under vacuum to give a light yellow polymer, **5** (0.047 g, 94%). $M_n^{NMR} = 5200$ g/mol, $M_n^{GPC} = 4400$ g/mol, $M_w/M_n = 1.34$. IR ($\nu_{max}$/cm$^{-1}$): 2976, 2911, 1724, 1478, 1446, 1392, 1367, 1253, 1229, 1140, 1113, 1029, 928, 844, 766, 750. $^1$H NMR ($CDCl_3$, 500 MHz): $\delta$ 1.27−1.50 (br, (C$H_3$)$_3$C), 1.24−1.72 (br, C$H_2$ of the polymer backbone), 1.72−1.92 (br, C$H_2$ of the polymer backbone), 2.15−2.42 (br, C*H* of the polymer backbone), 4.40 (br s, C$H_2$SPh in end group), 4.45 (s, C$H_2$OCH$_2$ in end group), 4.55 (s, CH$_2$OC$H_2$ in end group), 6.74−7.18 (m, Ar*H* in end groups). $^{13}$C NMR ($CDCl_3$, 500 MHz): $\delta$ 21.2 (*C*H$_3$CHCH$_3$ on the chain end), 25.4−25.7 ((*C*H$_3$)$_3$C on the side chain), 34.2−34.4 (carbon on the polymer backbone), 41.7−42.1 (carbon on the polymer backbone), 80.3 ((CH$_3$)$_3$*C* on the polymer side chain), 125.7 ((CH$_3$)$_3$*C*−O) on the polymer side chain), 125.5−135.8 (Ar*C*, SPh on the chain ends), 151.5 (Pd−*C* on chain end) 173.6−173.8, (*C*═O on the polymer side chain). UV/vis (DMF): $\lambda_{max} = 350$ nm.

**Deprotection of Metal-Complexed P$^t$BuA 5 To Give Metal-Complexed PAA 6.** To a 100 mL, round-bottom flask equipped with a stir bar was added **5** ($M_n^{NMR} = 5200$ g/mol, 0.100 g, 0.019 mmol), followed by dry dichloromethane (5 mL). The mixture was allowed to stir for 30 min to dissolve the polymer and then cooled to 0 °C. Trifluoroacetic acid (TFA, 0.918 g, 8.04 mmol) was then added at 0 °C. After the mixture was allowed to stir overnight at room temperature, the dichloromethane and excess TFA were removed at room temperature by passing air through the flask overnight. The polymers were purified by dissolving in THF (10 mL) and water (10 mL), transferred to presoaked dialysis membrane tubes, and dialyzed against deionized water for 3 d. Lyophilization of the water solution inside the dialysis tubes gave **6** as a light brown solid (0.056 g, 97%). $M_n^{NMR} = 2900$ g/mol. $^1$H NMR (DMSO-$d_6$, 500 MHz): $\delta$ 1.0−2.3 (br, C*H* and C$H_2$ of polymer backbone), 4.35 (br s, C$H_2$SPh in end group), 4.19 (s, C$H_2$OCH$_2$ in end group), 4.28 (s, CH$_2$OC$H_2$ in end group), 6.68−7.16 (m, Ar*H* in end groups), 11.8−13.4 (br, COO*H*). $^{13}$C NMR (DMSO-$d_6$, 500 MHz): $\delta$ 124.2−136.3 (*C*, SPh on the chain ends), 152.5 (Pd−*C* on chain end). IR ($\nu_{max}$/cm$^{-1}$): 3500, 2800, 1941, 1875, 1712, 1601, 1583, 1493, 1452, 1235, 1171, 1115, 1068, 1029, 908, 878, 810, 758, 698, 539. UV/vis (DMF): $\lambda_{max} = 350$ nm.

**Amphiphilic Block Copolymer Formation, 7.** Complexed poly(acrylic acid) (PAA) **6** ($M_n^{NMR} = 2900$ g/mol, 0.050 g, 0.17 mmol), and pyridine end-functionalized PS **4** ($M_n^{NMR} = 3600$ g/mol, $M_n^{GPC} = 2400$ g/mol, $M_w/M_n = 1.18$; 0.069 g, 0.17 mmol), were dissolved in *N*,*N*-dimethylformamide (DMF, 10 mL). The mixture was allowed to stir for 4 h under ambient conditions. Removal of the solvent under vacuum afforded **7** as a brown solid (0.119 g, 100%). $M_n^{NMR} = 6700$ g/mol. $^1$H NMR (DMF-$d_7$, 500 MHz): $\delta$ 1.22−1.70 (br, C$H_2$ of the polymer backbone), 1.74−2.04 (br, C$H_2$ of the polymer backbone), 2.15−2.41 (br, C*H* of the polymer backbone), 4.20 (s, C$H_2$OCH$_2$ in end group), 4.26 (s, CH$_2$OC$H_2$ in end group), 4.48 (Br s, C$H_2$SPh in end group), 6.20−7.30 (m, Ar*H* in side chain), 7.11−7.27 (m, Ar*H* in end groups), 8.16−8.26 (m, co-ord α pyr Ar*H*). $^{13}$C NMR (DMF-$d_7$, 500 MHz): $\delta$ 26.8−43.8 (polymer backbone *C*), 124.2−136.4 (*C*, SPh on the chain ends), 175.9 (*C*═O on side chain). IR ($\nu_{max}$/cm$^{-1}$): 3500, 2800, 1941, 1875, 1712, 1601, 1583, 1493, 1452, 1235, 1171, 1115, 1068, 1029, 908, 878, 810, 758, 698, 539. UV/vis (DMF): $\lambda_{max} = 350$ nm.

**Micellization of Amphiphile 7 To Afford 8.** A round-bottom flask equipped with a stir bar was charged with **7** (0.120 g, 0.018 mmol), and DMF (120 mL) was added. The solution was allowed to stir at room temperature for 1 h to ensure the mixture was homogeneous and that all of the polymer was dissolved. Deionized nanopure water (130 mL) was added via a metering pump at the rate of 10 mL/ h. After all of the water had been added, the opaque micelle solution was transferred to dialysis tubing (MWCO ≈ 3.5 kDa) and dialyzed against deionized nanopure water exhaustively to remove all of the DMF. The final volume of **8** was 390 mL, affording a polymer concentration of ca. 0.31 mg/mL. $D_h$(DLS) = 79 ± 1 nm; $\zeta = -52 \pm 1$ mV; $D_{av}$(TEM) = 54 ± 5 nm; $D_{av}$(AFM) = 78 ± 12 nm; $H_{av}$(AFM) = 2.6 ± 0.6 nm. UV/vis (H$_2$O): $\lambda_{max}$ = 350 nm. Lyophilization of a portion of this solution gave **8** as a light brown solid.

**Shell Cross-Linking of Micelle 8 To Give Nanoparticle 9.** To a stirred solution of micelle **8** (100 mL, 0.31 mg/mL) in a round-bottom flask was added, dropwise over 10 min, a solution of 2,2′-(ethylenedioxy)bis(ethylamine) (0.000082 g, 0.00055 mmol) in deionized water (2 mL). The solution was allowed to stir for 2 h at room temperature. To this reaction mixture was added dropwise, via a metering pump at the rate of 15 mL/h, a solution of 1-[3′-(dimethylamino)propyl]-3-ethylcarbodiimide methiodide (0.0003 g, 0.0011 mmol) dissolved in deionized water (1 mL). The reaction mixture was allowed to stir overnight at room temperature, transferred to presoaked dialysis membrane tubes (MWCO ≈ 3.5 kDa), and dialyzed against deionized water for 4 d to remove small-molecule contaminants. The final volume of **9** was 160 mL, affording a polymer concentration of ca. 0.30 mg/mL. $D_h$(DLS) = 71 ± 1 nm; $D_g$(SLS) = 54 nm, $\zeta = -25 \pm 1$ mV; $D_{av}$(TEM) = 48 ± 4 nm; $D_{av}$(AFM) = 66 ± 6 nm; $H_{av}$(AFM) = 4.4 ± 1.0 nm. UV/vis (H$_2$O): $\lambda_{max}$ = 350 nm. Lyophilization gave **9** as a light brown solid.

**Hollowing-Out of Nanoparticle 9 To Give Nanocage 10.** Nanoparticle **9** (30 mL) was dialyzed against THF/water (1:4) to swell the hydrophobic core for 1 d. This solution was then dialyzed against a 10 mM phosphate buffer solution, pH = 5.0, for 4 d to cleave the metal−hydrophobic chain bond. The resultant solution was then exhaustively dialyzed against a THF/water (1:4) solution for 4 d to remove the core and then dialyzed into nanopure water exhaustively for 4 d, to remove all of the THF (all dialysis tubing was MWCO ≈ 12−14 kDa). The final volume of **10** was 30 mL, affording a polymer concentration of ca. 0.30 mg/mL. $D_h$(DLS) = 94 ± 1 nm; $D_g$(SLS) = 101 nm; $\zeta = -33 \pm 2$ mV; $D_{av}$(TEM) = 74 ± 7 nm; $D_{av}$(AFM) = 139 ± 11 nm; $H_{av}$(AFM) = 1.5 ± 0.4 nm. UV/vis (H$_2$O): $\lambda_{max}$ = 350 nm. Lyophilization gave **10** as a light brown solid.

***Scheme 1.*** Synthesis of NMP Initiators (a) **1** and (b) **2**

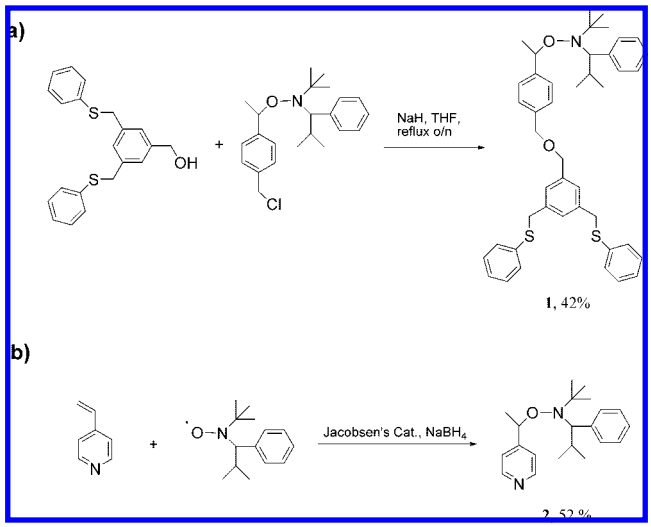


## 3. Results and Discussion

We first incorporated an SCS pincer ligand onto a chloro-functionalized NMP initiator to make a novel SCS pincer NMP initiator, **1**, which could potentially facilitate Heck catalysis when complexed to a Pd(II) metal center and bound to a polymer support. This has been reported previously by Weck and co-workers for similar Pd−pincer complexes.[29,34–36] The complexation of this ligand is well known for pyridine functionalities,[32,37,75] and to utilize this unsymmetrical Pd(II) binding system in block copolymer self-assembly, we synthesized a novel pyridyl-functionalized NMP initiator, **2**, which would complex to the Pd metal center in the pincer complex.[75]

The SCS pincer ligand, bearing a pendant alcohol, and the chloro-NMP universal initiator were reacted, forming the target SCS pincer ligand-functionalized NMP initiator **1** using sodium hydride as a strong base (Scheme 1a). Upon reaction completion, any excess sodium hydride was quenched by adding acetic acid dropwise to the reaction mixture. The product was then separated from the starting materials by flash chromatography, yielding **1** as a light yellow gum in a 42% yield. The $^1$H NMR spectrum of **1** shows all of the diastereomeric proton peaks associated with the product SCS-functionalized NMP initiator.[86] The $^1$H NMR spectrum revealed that there were no peaks at $\delta = 4.60$ for the C$H_2$Cl or C$H_2$OH methylene protons of the two starting materials. The new ether linkage protons of **1** (C$H_2$OC$H_2$) were observable as two inequivalent proton environments as singlets at $\delta$ 4.44 and 4.45, which both integrate to two protons. The structure of **1** was confirmed by elemental analysis, and the $^{13}$C NMR spectrum of **1** shows distinctive peaks such as two ether linkage carbon shifts at $\delta$ 72.2 and 72.1 and the central aromatic ring carbon *ortho* to the C$H_2$SPh groups at $\delta$ 138.8.

A second ligand-NMP initiator was synthesized with a pendant pyridine moiety, **2**, using a method similar to that reported in the literature (Scheme 1b).[86] The novel initiator **2** was synthesized in a 52% yield, and the structure was confirmed by $^1$H and $^{13}$C NMR analysis. In the $^1$H NMR spectrum of **2**, nearly identical shifts are observed for the diastereomeric peaks on the nitroxide fragment which are found for end-group signals attributable to **1**. However, structurally indicative peaks for **2** are observable as a broad multiplet at $\delta$ 8.60, accounting for two pyridine ring protons α to the *para* ring nitrogen atom. The proton added as a hydride from $NaBH_4$ across the olefinic fragment can be observed in its new environment adjacent to the nitroxide fragment and aromatic ring as a doublet at $\delta$ 1.27. The $^{13}$C NMR spectrum of **2** shows a distinctive peak for the carbons α to the pyridine nitrogen at $\delta$ 149.8. Further structural confirmation of **2** was indicated by elemental analysis, and LC-MS showed a 100% peak for the molecular ion at ca. 326.5 Da.

***Scheme 2.*** Polymerization Conditions of $^t$BuA Using Initiator **1**

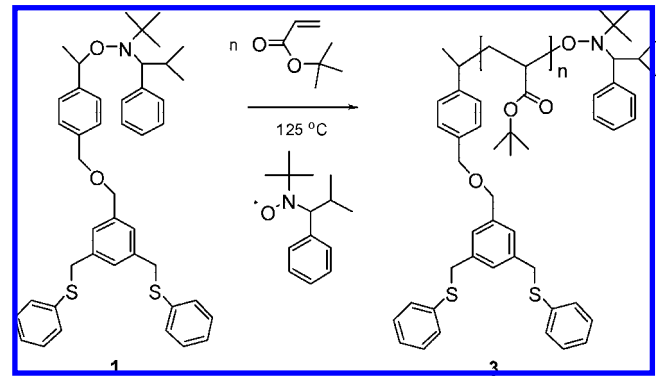


***Table 1.*** $^t$BuA Polymerization Data Using Initiator **1** at 125 °C, Bulk

| [M]:[**1**]:[free nitroxide] | time (h) | $M_n$(NMR) | $M_n$(GPC) | $M_w/M_n$ |
|---|---|---|---|---|
| [200]:[1]:[0.05] | 116 | 25 600 | 24 600 | 1.20 |
| [100]:[1]:[0.05] | 95 | 7 800 | 9 800 | 1.22 |
| [50]:[1]:[0.05] | 46 | 4 500 | 5 200 | 1.14 |

**Polymerization of *tert*-Butyl Acrylate Using Initiator 1.** The initiator **1** was utilized in the NMP of $^t$BuA at 125 °C in the presence of free nitroxide. This afforded polymers with controlled molecular weight and polydispersity, as is expected for the NMP of acrylates (Scheme 2). For the eventual formation of the metallodiblock copolymer, theoretical degrees of polymerization (DPs) of 50, 100, and 200 were targeted, which can be achieved by altering the monomer-to-initiator ratio and the polymerization time to access various conversions (Table 1).

It has been reported that, for the controlled polymerization of acrylates using NMP techniques, an excess of free nitroxide is required;[84] thus, 5 mol % of free nitroxide was added to push the equilibrium in favor of dormant chains to increase the control over the polymerization. The kinetics for the NMP of $^t$BuA initiated by **1** ($k_p = 4.0 \times 10^{-4}$ min$^{-1}$) in the presence of free nitroxide were slower than those reported by Hawker and co-workers[86] for the NMP of $^t$BuA using a nonfunctional alkoxyamine initiator in the presence of free nitroxide. In addition, an apparent induction period of ca. 8 h was observed, but after this time a linear relationship between $\ln([M]_0/[M])$ versus time was observed (Figure 1a), indicating no detectable termination occurring in this system.

Good agreement between the molecular weights of the resultant polymers as determined by NMR and GPC analysis was observed, indicating no unfavorable interaction on the GPC column of the thio-phenyl moieties and excellent end group fidelity (Figure 1b).

Figure 1b also shows a good linear dependence of molecular weight with respect to percentage conversion, which is a key feature of a controlled radical polymerization. Importantly, the SCS ligand end group remained intact after the polymerization, as proven by extended $^1$H NMR spectroscopy; peaks corresponding to end-group ligand proton environments, such as the

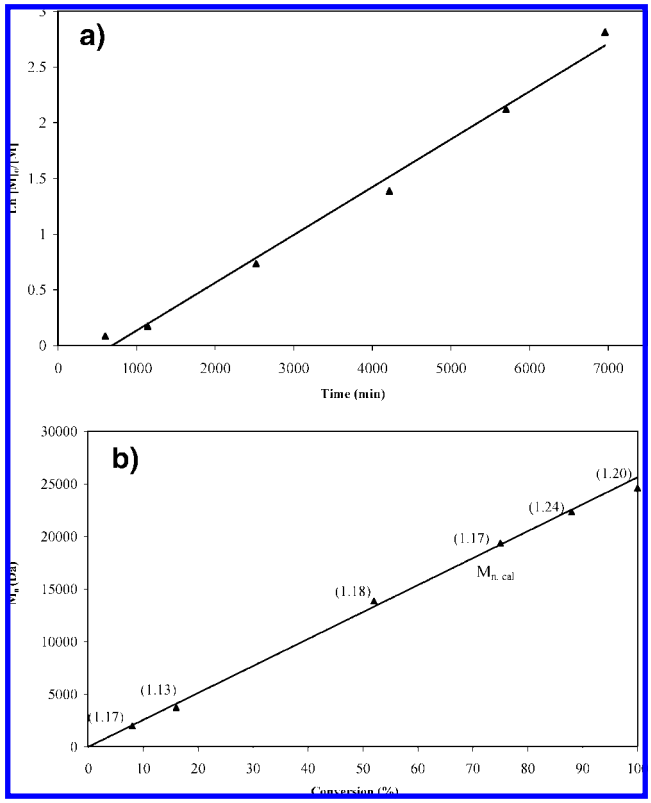


***Figure 1.*** (a) Kinetic plot for the NMP of $^t$BuA at 125 °C in bulk with initiator **1**, [M]:[1]:[free nitroxide] = [200]:[1]:[0.05]. (b) Plot of molecular weight [$M_n$(GPC)] against conversion; the trendline is $M_{n,theor}$(NMR), with polydispersity in parentheses.

***Scheme 3.*** Polymerization of Styrene Using Pyridyl-Functionalized NMP Initiator **2**

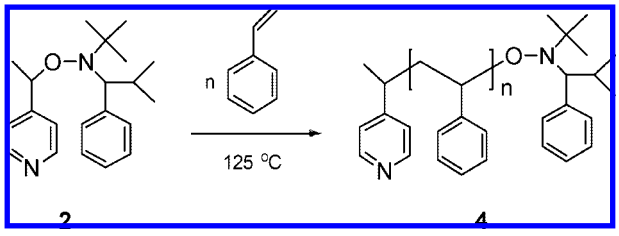


$CH_2OCH_2$ methylene signals at $\delta$ 4.45 and 4.44 and $CH_2SPh$ at $\delta$ 4.01, were found for all P$^t$BuA polymers and were integrated with respect to broadened polymer backbone signals and side-chain *tert*-butyl signals in the region $\delta$ 1.00−2.50. From this, a theoretical DP could be calculated by comparing end group to polymer chain integrals, and hence $M_n$(NMR) could be calculated and showed good agreement with values calculated by GPC analysis, which indicated that excellent end-group fidelity is achieved during the polymerization. Extended $^{13}$C NMR spectroscopy shows the presence of SPh phenyl ring carbons in the region $\delta$ 125.5−135.7, showing further evidence for the functional end group.

**Polymerization of Styrene Using Initiator 2.** The NMP initiator **2** (Scheme 3) provided similar control, initiating the NMP of styrene at 125 °C, affording polymers with predictable molecular weights and low polydispersities, as is expected for the NMP of styrene derivatives.[86] The results of the polymerization at various conversions are summarized in Table 2.

A linear kinetic relationship of ln([M]$_0$/[M]) versus time ($k_p$ = 2.8 × 10$^{-3}$ min$^{-1}$) was observed for this system, with no induction period observed, indicating a controlled polymerization process with minimal termination occurring (Figure 2a). A plot of theoretical $M_n$(NMR) versus conversion (Figure 2b) shows that the molecular weights determined by GPC measurements showed good agreement with theoretical molecular weights. However, the molecular weights determined by GPC measurements for pyridine end-functionalized PS show a consistent shift below theoretical values obtained from the NMR spectrum, indicating an unfavorable interaction of the pyridine moiety at the end of these polymers on the GPC column, as reported previously for terpyridine end-functionalized polymers.[26]

***Table 2.*** Bulk NMP of Styrene Using Initiator **2**, Using 200 equiv of Monomer Relative to **2** at 125 °C

| time/ h | conv (%) | $M_{n,theor}$(NMR) | $M_n$(GPC) | $M_w/M_n$ |
|---|---|---|---|---|
| 1 | 19 | 4 000 | 2 800 | 1.28 |
| 2 | 32 | 6 700 | 5 100 | 1.21 |
| 3 | 41 | 8 500 | 7 000 | 1.17 |
| 4 | 49 | 10 200 | 8 600 | 1.15 |
| 6 | 63 | 13 100 | 10 800 | 1.13 |
| 11 | 95 | 19 800 | 17 700 | 1.19 |

A low-molecular-weight pyridine chain-end-functionalized PS block was analyzed using MALDI-ToF mass spectrometry. Figure 3 shows the MALDI-ToF mass spectrum of PS, in which separate oligomers are clearly resolved and separated by *m*/*z* 104, corresponding to the mass of styrene. This family of peaks corresponds to the expected product, where one end is pyridyl-functionalized and the other end is functionalized with the free nitroxide fragment from the initiator. MALDI-ToF mass spectrometry thus further supports the end-group fidelity of the pyridyl functionality of the PS blocks.

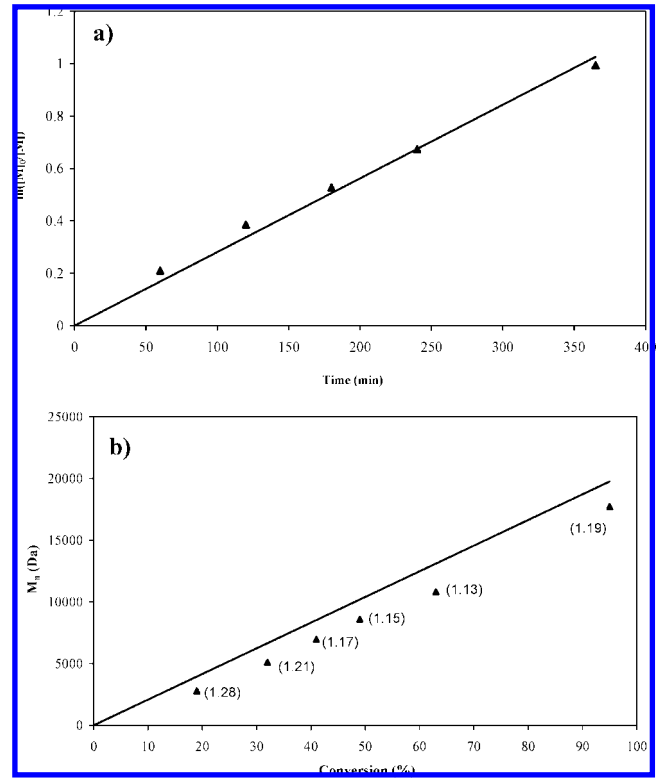


***Figure 2.*** (a) Kinetic plot for the NMP of styrene at 125 °C in bulk with initiator **2**, [M]:[**2**] = [200]:[1]. (b) Plot of molecular weight [$M_n$(GPC)] against conversion; the trendline is $M_{n,theor}$(NMR), with polydispersity in parentheses.

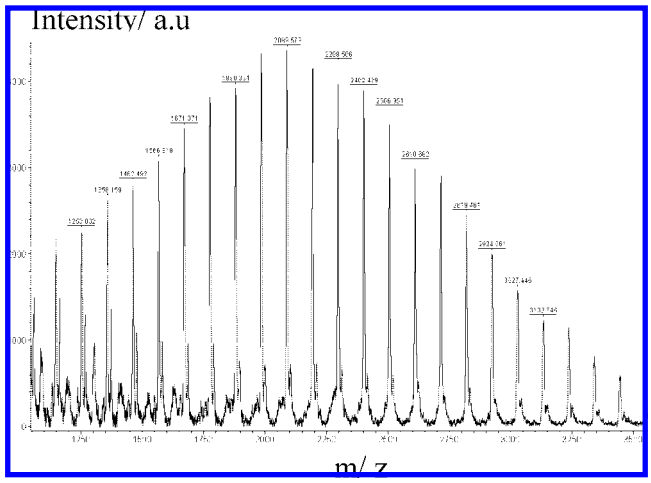


***Figure 3.*** MALDI-ToF MS of pyridyl-functionalized polystyrene block **4**, run in a dithranol matrix with silver trifluoroacetate cationizing agent.

**Preliminary Metal Complexation Experiments of SCS NMP Initiator 1.** To establish a straightforward route toward the palladium(II) complexation of chain-end-functionalized P$^t$BuA/PAA polymers, first the palladium(II) complex of the SCS pincer NMP initiator **1** was synthesized. This proceeded by refluxing **1** in acetonitrile with a presynthesized palladium precursor complex, *trans*-[Pd(PhCN)$_2$Cl$_2$], as reported previously in the literature.[76] The chloro-Pd(II) complex of **1** showed a distinctive Pd−C shift at $\delta$ 149.5 in the $^{13}$C NMR spectrum, indicating successful palladation at the carbon *ortho* to the pincer "arms", which is consistent with the literature for similar SCS-based Pd(II) complexes.[77] No evidence of the original *ortho* carbon signal at $\delta$ 138.2 indicated complete metal insertion. In addition, the Pd(II) complex gave a distinctive metal-to-ligand charge-transfer (MLCT) band at $\lambda \approx 350$ nm in the UV−vis spectrum.

However, a route toward palladium(II) complexation was required which would allow for the more facile displacement of the pendant ligand by a pyridine functionality. To obtain such a complex, **1** was reacted with a more labile precursor Pd complex, commercially available [Pd(MeCN)$_4$(BF$_4$)$_2$], at room temperature in acetonitrile.[75] This complex also showed a distinctive Pd−C shift in the $^{13}$C NMR spectrum at $\delta$ 151.2.[77] Evidence for the complete complexation of **1** was provided by $^1$H NMR spectroscopy due to complexed diastereotopic C$H_2$SPh proton signals appearing downfield-shifted by $\delta$ 0.5 from the signals for the uncomplexed ligand, to $\delta$ 4.60. Their was no evidence for the presence of the original singlet for uncomplexed C$H_2$SPh proton signals at $\delta$ 4.1, indicating complete metal complexation. The shifted complexed signal is also significantly broadened due to the slow conformational interconversion of the Pd(II)-containing five-membered ring. These observations are consistent with those reported in the literature.[75] There is also an upfield shift for the ether linkage protons of **1**, C$H_2$OC$H_2$, from ca. $\delta$ 4.45 to ca. $\delta$ 4.34, and no evidence of the original signal.

**Preliminary Investigations To Complex NMP Initiators 1 and 2.** The facile complexation route with [Pd(MeCN)$_4$(BF$_4$)$_2$] produced the charged Pd(II) complex of **1**, bearing an acetonitrile (MeCN) ligand, which was found to undergo ligand displacement with the pyridine-functionalized initiator **2** to form the desired complex after stirring in chloroform at room temperature for only 5 min. This proved to be straightforward, since the pendant MeCN ligand is particularly labile toward substitution, which facilitated its displacement by the pyridine moiety on initiator **2**. A similar ligand-exchange experiment with **2** using the SCS pincer complex starting material bearing a chloro ligand proceeded in such a facile manner only when the chloro species was pretreated with silver triflate. This produced the visible precipitation of silver chloride as a consequence of the abstraction of the chloride ligand from the complex, after which the naked palladium(II) metal ion formed readily underwent complexation with **2**.

Both complexation routes were followed by $^1$H NMR spectroscopy, and nearly identical shifts were observed for both reactions. A $^1$H NMR spectrum of the reaction mixture showed an upfield shift of the α proton peaks on the pyridine ring from $\delta$ 8.60 (uncoordinated) to $\delta$ 8.15 (coordinated), observable after only 5 min of stirring at room temperature in $CDCl_3$.[75] This shift of the α proton peaks is due to the ring current shielding effect of the phenyl rings (on the sulfur atoms of the pincer ligand) when the pyridine ligand is complexed to the Pd metal center. The α proton peaks are also broadened, suggesting hindered rotation of the pyridine ligand with respect to the plane of coordination,[75] consistent with literature reports. Small peaks at $\delta$ 8.60 were still observable in the $^1$H NMR spectrum, suggesting that uncomplexed pyridine ligand was still present in solution. However, this observation may be explained by a slow exchange of pyridine and a coordinating solvent (such as $CDCl_3$) on the NMR time scale, consistent with literature reports[75] for similar complexation experiments for SCS−Pd(II)−pyridine systems.

**Metal Complexation of Poly(*t*BuA) Block 3 To Give 5.** The complexation of the SCS pincer ligand-functionalized P$^t$BuA **3** proceeded in nearly quantitative yields to give **5** after stirring with a [Pd(MeCN)$_4$(BF$_4$)$_2$] precursor complex overnight at room temperature in acetonitrile (Scheme 4). The complexation of **3** was similar to that for **1**, although longer reaction times were required to enable complete complexation of the polymer blocks. Complexation appeared to have gone to completion from extended $^1$H and $^{13}$C NMR spectroscopy studies, showing only complexed proton signals and no uncomplexed peaks by comparison with model complexation experiments with the initiator **1**.[75] The observable shifts were consistent with the Pd(II) complex of **1,** and the complexed polymer **3** also showed the distinctive MLCT band at $\lambda \approx 350$ nm in the UV−vis spectrum in THF.

**Deprotection of 5 To Give Pd-Complexed PAA 6.** Cleavage of the *tert*-butyl ester groups in the complexed P$^t$BuA **5** to form metal-complexed PAA **6** was achieved by treating **5** with anhydrous TFA in dichloromethane at room temperature overnight (Scheme 4). Infrared spectroscopy was used to monitor the progress of the reaction and also to confirm that the deprotection of all the ester groups had gone to completion. The IR spectra of **6** displayed a shift in the carbonyl stretch from $\nu \approx 1720$ cm$^{-1}$ in **5** to 1705 cm$^{-1}$ with a distinctive broadening of the peak, indicative of carboxylic acid carbonyl stretching. Also evident from the IR spectra of **6** was the stretching associated with broad H-bonded carboxylic acid OH stretches at $\nu \approx 3175$ cm$^{-1}$, providing further evidence for ester deprotection. The integrity of the SCS pincer end-group complex in **6** after deprotection was crucial to the eventual formation of the diblock copolymer **7** from the constituent end-functionalized homopolymers **5** and **6**. Thus, an extended $^1$H NMR spectrum of **6** in DMSO-$d_6$ was used to show that the SCS complex was still intact after deprotection conditions. Indicative end complex peaks for coordinated C$H_2$SPh proton environments were still identifiable as a broad singlet at $\delta$ 4.65 and C$H_2$OC$H_2$

***Scheme 4.*** Complexation of P$^t$BuA **3** To Afford **5** and Deprotection To Give Complexed PAA **6**

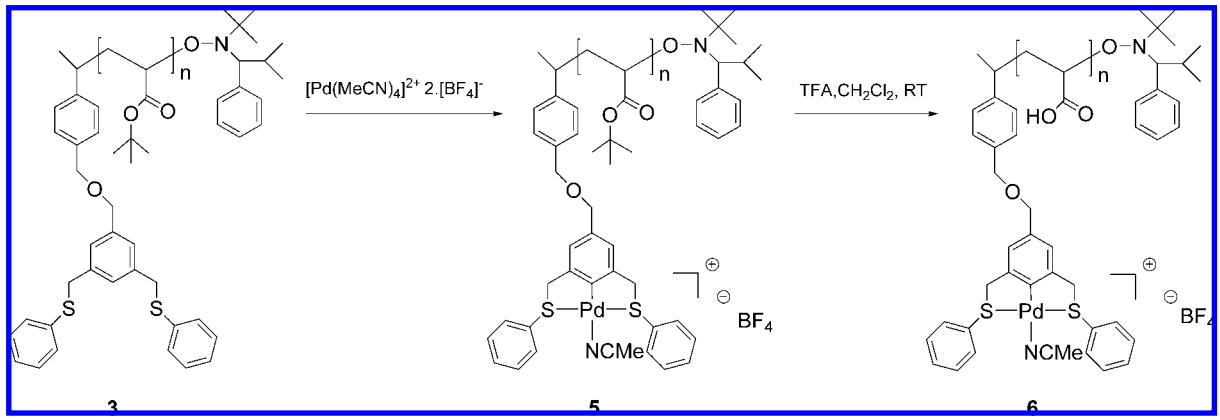


***Scheme 5.*** Synthesis of Palladium(II)-Complexed NCC Amphiphilic Diblock Copolymer **7**

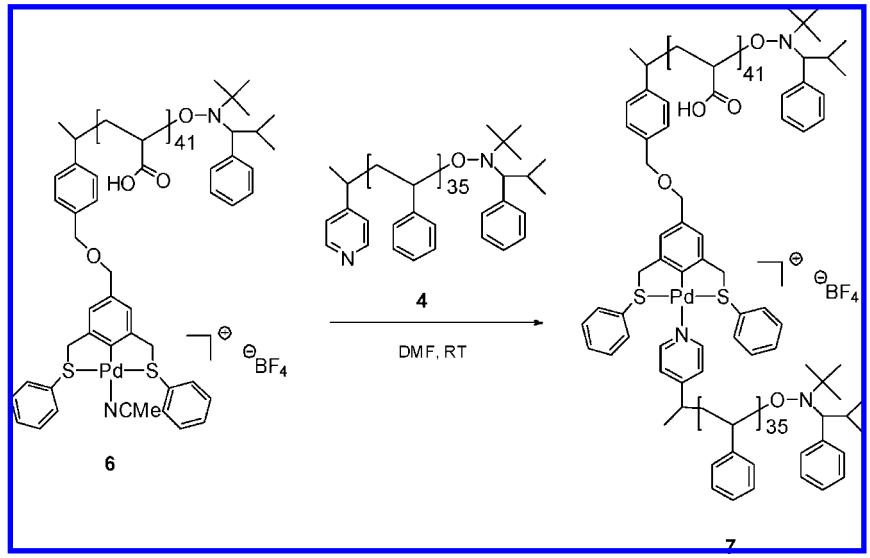


protons at $\delta$ 4.55, and when integrated with respect to side-chain acid proton integrals, these peaks gave a block length (DP) of ca. 40, as was found by extended $^1$H NMR spectroscopic measurements for **3**. The $^{13}$C NMR spectrum of **6** in DMSO-$d_6$ also showed distinctive Pd−C shifts associated with the end-group SCS complex at $\delta$ 150.3, and the complexed PAA polymer **6** also showed a distinctive MLCT band in the UV−vis spectrum in DMF.

**Amphiphilic Block Copolymer Formation from 4 and 6 To Give 7.** Equal molar equivalents of the metal-complexed PAA block **6** and pyridine end-functionalized PS block **4** were dissolved in DMF and stirred at room temperature (Scheme 5). The formation of the diblock copolymer was evident from $^1$H NMR spectroscopy, with the amphiphilic diblock copolymer **7** showing an upfield shift of the pyridine ring $\alpha$ proton peaks from $\delta$ 8.60 (uncoordinated) to $\delta$ 8.15 (coordinated) in the extended $^1$H NMR spectrum in DMF-$d_7$, indicating complexation of the two chain-end ligand functionalities and hence diblock copolymer formation.

**Micellization of 7 To Afford 8.** Micelles of narrow size distribution, **8**, composed of the block copolymer $PAA_{41}$-[Pd]-$PS_{35}$, **7** (0.120 g, 0.018 mmol), were formed by slow addition (10 mL/min) of an equal volume of nanopure water to a stirred solution of the diblock copolymer in DMF, followed by exhaustive dialysis against deionized water to remove the organic phase (Scheme 6). The well-defined structure of **8** in solution was evident from DLS measurements (80 ± 1 nm). The size and shape of NCCMs **8** were measured in the solid state by AFM and TEM (Figures 4 and 6). The results are summarized in Table 3.

**Cross-Linking of 8 To Afford NCCNs 9.** The hydrophilic shell of NCCMs **8** was selectively cross-linked to form NCCNs **9** (Scheme 6) using amidation coupling chemistry. This was achieved by activating a fraction of the carboxylic acid groups in the PAA shell with 1-[3′-(dimethylamino)propyl]-3-ethylcarbodiimide methiodide (0.25 equiv based upon the remaining acid functionalities), followed by reaction with a linker molecule, 2,2′-(ethylenedioxy)bis(ethylamine) (0.125 equiv based upon the remaining acid functionalities) overnight at room temperature. It has been suggested that 25% cross-linking was sufficient to ensure that robust and stable nanoparticles were formed that still maintain a high degree of permeability and hence enable removal of the core after shell stabilization to form nanocage **10**. Cross-linking was successful, as evidenced by a marked reduction in the hydrodynamic diameter $D_h$ of the nanoparticle (71 ± 1 nm) compared to that of the micelles (80 ± 1 nm), as measured by DLS analysis. This is consistent with literature reports for covalently bonded PAA-*b*-PS micelle/nanoparticle systems. Zeta potential measurements, as determined by electrophoretic light scattering, were all negative and indicate, as expected, a negative charge on the surfaces of the micelles and nanoparticles. The micelle $\zeta$ values were more highly negative than were those values measured for their nanoparticle

***Scheme 6.*** (i) Micellization of Amphiphilic Diblock Copolymer **7** To Afford NCCMs **8**; (ii) Covalent Cross-Linking in the Outer Shell To Afford NCCNs **9**; and (iii) Core Removal To Give Nanocages **10**

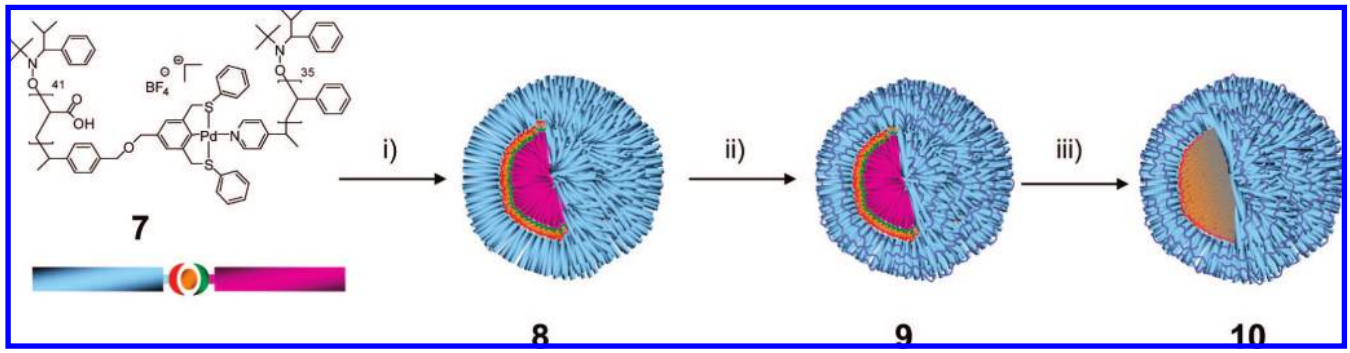


***Table 3.*** Characterization Data for NCCMs **8** and the Corresponding NCCNs **9** and Nanocages **10**

| | DLS | AFM | | TEM | zeta |
|---|---|---|---|---|---|
| particle | $D_h$[a] (nm) | $D_{av}$[b] (nm) | $H_{av}$[b] (nm) | $D_{av}$[c] (nm) | $\zeta$[d] (mV) |
| **8** | 80 ± 1 | 78 ± 12 | 2.6 ± 0.6 | 54 ± 5 | −52 ± 1 |
| **9** | 71 ± 1 | 66 ± 6 | 4.4 ± 1.0 | 48 ± 4 | −25 ± 1 |
| **10** | 94 ± 1 | 139 ± 11 | 1.5 ± 0.4 | 74 ± 7[e] | −33 ± 2 |

[a] Number-averaged hydrodynamic diameters of particles in aqueous solution by DLS. [b] Average heights and diameters of particles were measured by tapping-mode AFM, calculated from the values for ca. 100 particles. [c] Average diameters of particles were measured by TEM, calculated from the values for ca. 150 particles. [d] Zeta potential, from 16 determinations of 10 data sets. [e] Note that particles no longer appear to be spherical by TEM analysis.

counterparts, thus supporting the synthetic transformation occurring in the shell layer of the micelle upon consumption of carboxylate groups during cross-linking to the nanoparticle (Table 3). The size and shape of the NCCNs **9** were measured in the solid state by AFM and TEM. As previously observed for related nanostructures, the NCCNs in this study deform to a lesser extent on the carbon-coated TEM grid than they do on the mica substrate which was utilized for AFM.[90]

**Hollowing-Out PS Core of 9 To Afford 10.** NCCNs **9** were hollowed out by removal of the PS core domain via cleavage of the pyridine−palladium noncovalent bond at the core−shell interface (Scheme 6). This was achieved through protonation of the pyridine moiety on the chain end of the PS blocks at low pH. However, initial dialysis of **9** in a 1:4 THF/$H_2O$ solvent mixture was necessary to swell and solubilize the hydrophobic core to aid removal. The THF/$H_2O$ solution of **9** was then dialyzed exhaustively in a 10 mM HCl buffer solution (pH 5.0) to protonate the pyridine end group. The solution was then dialyzed extensively in 1:4 THF/$H_2O$ to remove all of the free PS chains (care was taken to ensure that high-molecular-weight dialysis tubing was utilized to facilitate transport of the polymer chains through the membrane). This polymer solution was then dialyzed exhaustively in deionized water for 4 days, incorporating 20 water changes. The loss of the PS core was inferred by the DLS analysis of the newly formed nanocages **10** due to a significant increase in the hydrodynamic diameter in solution (94 ± 1 nm) from the micelle and the nanoparticle. This increase is indicative of the PAA chains being more spatially extended in solution, since there is now no hydrophobic interior (no hydrophobic effect) constricting their extension in aqueous solution. The size and shape of the core-hollowed nanoparticles or nanocages **10** were measured in the solid state by AFM and TEM; the results are summarized in Table 3. A representative TEM image of **10** is shown in Figure 5, and representative AFM images of **9** and **10** are in Figure 6. It is clear from Figure 5 that relatively well-defined nanostructures are still present in solution, although their size has increased markedly and they appear to be less spherical than the parent micelles and nanoparticles. Figure 6 highlights the decrease in height upon removal of the glassy PS core upon nanocage formation. A clearly flattened polymer ring can be observed which is proposed to

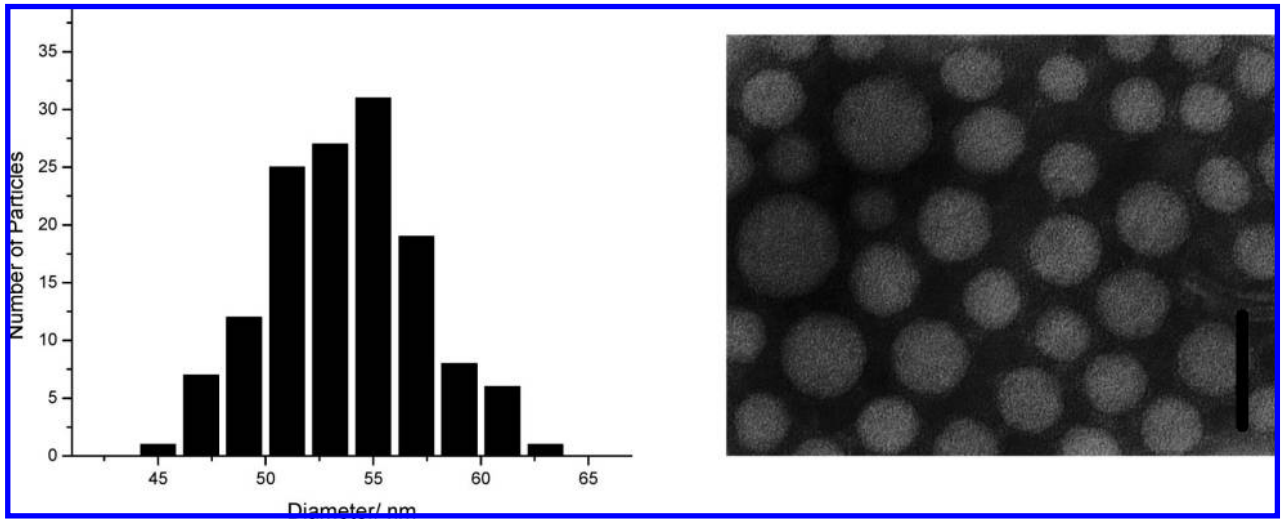


***Figure 4.*** Histogram showing the size distribution of the NCCMs **8** by TEM and a representative TEM image of **8** obtained by drop-depositing solutions on carbon grids and staining with phosphotungstanic acid. TEM scale bar = 100 nm.

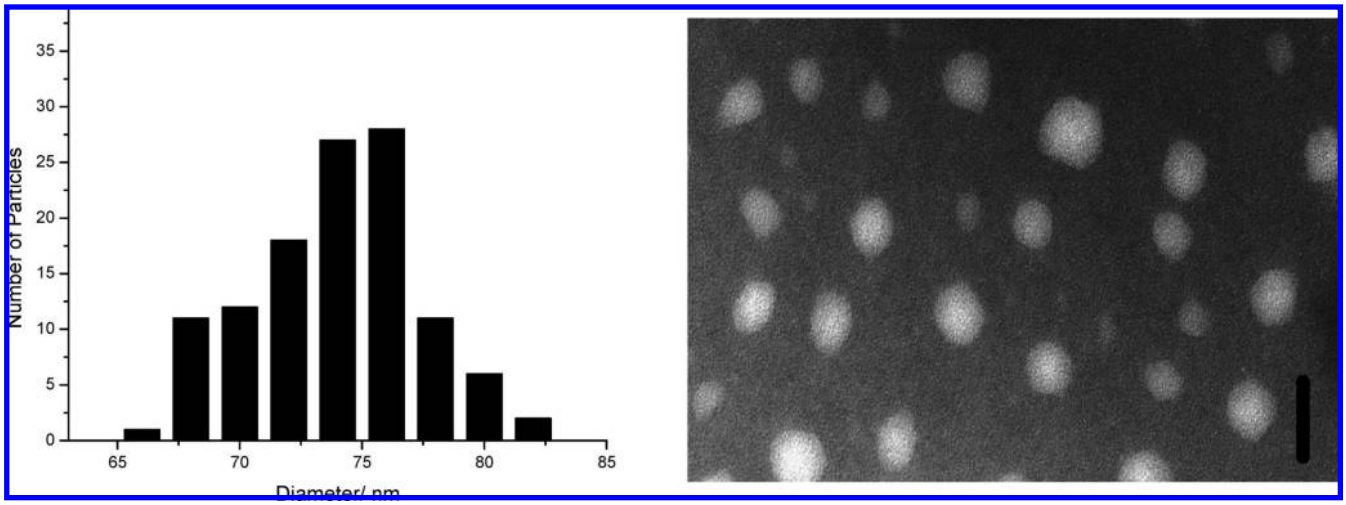


***Figure 5.*** Histogram showing the size distribution of the nanocages **10** by TEM and a representative TEM image of **10** obtained by drop-depositing solutions on carbon grids and staining with phosphotungstanic acid. TEM scale bar = 100 nm.

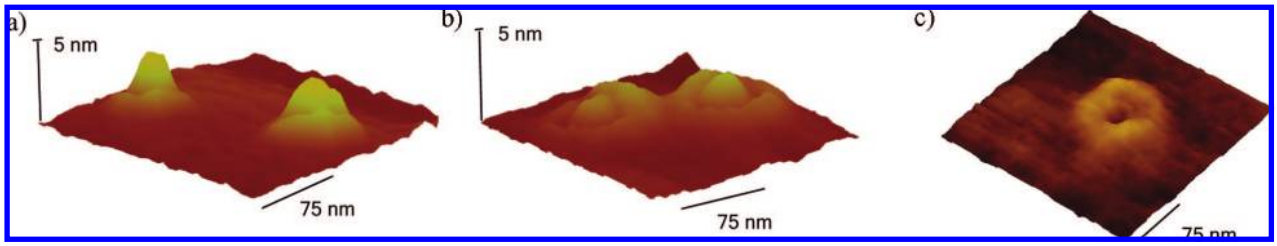


***Figure 6.*** Representative tapping-mode AFM images of (a) NCCNs **9**, (b) nanocages **10**, and (c) nanocages **10** after further dialysis. The solutions were drop-deposited onto freshly cleaved mica and allowed to dry under ambient conditions.

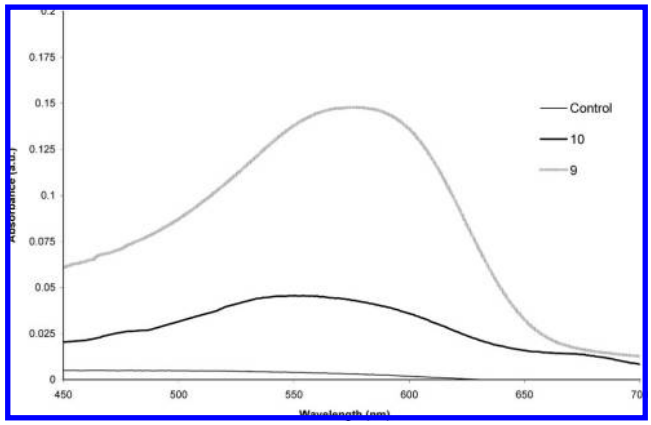


***Figure 7.*** UV−vis spectrum demonstrating the different sequestration abilities of the nanocage **10** and nanoparticle solution **9** with Nile red.

represent the PAA cage, yet a small central nodule within this ring was also visible which may be a result of incomplete removal of the PS core domain. Despite this, the AFM images obtained for nanocage **10** suggest that these two domains are no longer covalently connected. This was confirmed by further dialysis of the nanocage solution for 4 days, which allowed for the complete removal of the PS core domain (Figure 6c). Further work is currently underway to explore in more detail the excavation of the core domain and improve its efficiency. UV−vis analysis of the resultant solution demonstrated the characteristic signal (at ca. 350 nm, as was observed in the parent micelles and nanoparticles) attributable to the Pd, thus indicating that the metal center is still complexed within the nanocage after core removal. A 10-mL portion of the NCCNs **9** and the nanocages **10** was lyophilized and redissolved in 1.5 mL of 70:30 $D_2O$/THF-$d_8$. An extended $^1H$ NMR spectrum was run on both samples in the presence of deuterated THF to swell any PS in the core domain of either **9** or **10**. The $^1H$ NMR spectrum of **9** clearly showed the presence of aryl signals corresponding to PS (from $\delta$ 6.20 to 7.30) and signals attributable to cross-linked PAA, whereas the $^1H$ NMR spectrum of **10** did not show any signals in the aromatic region corresponding to PS ($\delta$ 6.2−7.3) but did show the presence of cross-linked PAA domain.

To further confirm the hollow nature of the particles **10**, SLS measurements were performed to determine the average radius of gyration, $R_g$. The ratio $R_g/R_h$ is useful for analyzing the structure of a particle, as ratios equal or greater than 1 indicate that a hollow particle has been formed.[91] The $R_g/R_h$ ratio for the parent nanoparticle was ca. 0.8, which is consistent with a spherical micelles structure, and after core excavation the nanocage **10** had an $R_g/R_h$ ratio of ca. 1.1. This clearly supports the formation of a hollow cage-like structure.

One expected difference between the parent NCCN and its derived nanocage is the ability of the NCCN to uptake hydrophobic guest molecules as a result of its amphiphilic character and hydrophobic core domain. Thus, the removal of the core domain in NCCN **9** to afford a hollow hydrophilic nanocage was expected to have a significant effect on the sequestration ability of nanostructure **10**. Nile red (9-diethylamino-5*H*-benzo[α]phenoxazine-5-one) was chosen, given its absorbance in a region (ca. 550 nm) of the spectrum which is far removed from the absorbances due to the polymer or nanostructure (around and below 300 nm). This was achieved experimentally using previously reported techniques.[66] Equivalent molar amounts of **9** and **10** were incubated overnight with

a large excess of Nile red, residual dye was removed by filtration through a 0.45-$\mu$m Teflon membrane, and the UV−vis spectrum was recorded for each solution (Figure 7). A control experiment using only water showed no significant absorbance after filtration, and this resultant absorbance reading was used as a background for subsequent measurements of **9** and **10**. The nanocage **10** showed little uptake of the hydrophobic guest compared to the parent nanoparticle, confirming that core excavation had been moderately successful.

## Conclusions

Synthetic strategies for the preparation of novel NCCM, NCCN, and functional core-hollowed nanostructures (nanocages) have been developed. To obtain these structures, a novel synthetic strategy has been developed using the chain-end functionalization of homopolymer blocks which have been assembled to afford unsymmetrical amphiphilic metallodiblock copolymers which can be further self-assembled to form well-defined micelles and nanoparticles. Utilizing a range of techniques such as SLS, DLS, AFM, and TEM analysis, we have shown that architectures produced utilizing this noncovalently connected diblock strategy are directly analogous to covalently connected micelles/nanoparticles and that the synthetic methodology toward them is just as facile. From the noncovalently connected nanoparticles, hollow cage-like structures could be prepared using extremely mild techniques to partially excavate the core domain while ensuring the metal center is still present within the nanostructure. These novel metal-functionalized nanocages were found to be highly hydrophilic and demonstrated significantly reduced uptake of hydrophobic guest molecules. Studies are underway to explore the availability of these metal centers within the nanostructures and their potential in pseudo-homogeneous supported Heck coupling reactions. Further work is also investigating the re-incorporation of hydrophobicity into the central core domain to allow for re-establishment of the amphiphilic character of the nanostructure and thus allow for the preparation of an internal cavity and confined hydrophobic environment within catalytically functionalized nanostructures.

**Acknowledgment.** The authors acknowledge the assistance of Mr. Matthew Stanford (University of Warwick) for MALDI-ToF MS analysis, Mr. Jared Skey and Dr. Jeremy Skepper (University of Cambridge) for TEM analysis, and Dr. Kevin Jackson (Wyatt Technologies) for SLS assistance. The authors thank Professor Sir Richard Friend (University of Cambridge) for valuable discussions and also thank the elemental analysis and mass spectrometry service (University of Cambridge) for their invaluable help. The authors thank the IRC in Nanotechnology, the Royal Society, and Downing College for funding.

JA800230K

(90) Huang, H.; Kowalswski, T.; Wooley, K. L. *J. Polym. Sci. Part A: Polym. Chem.* **2003**, *41*, 1659–1668.
(91) Burchard, W. *Adv. Polym. Sci.* **1983**, *48*, 1–124.